IEEE Access
Multidisciplinary | Rapid Review | Open Access Journal

SPECIAL SECTION ON THE INTERNET OF ENERGY: ARCHITECTURES, CYBER SECURITY, AND APPLICATIONS

Received January 29, 2017; accepted February 13, 2017, date of publication February 17, 2017, date of current version March 13, 2017.

Digital Object Identifier 10.1109/ACCESS.2017.2670526

A New Class of Highly-Miniaturized Reconfigurable UWB Filters for Multi-Band Multi-Standard Transceiver Architectures

MOHAMED KHEIR[1], THOMAS KRÖGER[2] AND MICHAEL HÖFT[3], (Senior Member, IEEE)

[1]RF-Development Team, IMS Connector Systems GmbH, 79843 Löffingen, Germany
[2]Bradken, Australia
[3]Institute of Electrical Engineering and Information Technology, Christian-Albrechts-University of Kiel, 24143 Kiel, Germany

Corresponding author: M. Kheir (m.s.kheir@gmail.com)

ABSTRACT Modern wireless communication systems typically employ multiple frequency bands for several standards. A new class of miniaturized ring filters with tuning capability is introduced for this purpose. The proposed filter structure is based on a single multi-mode resonator with variable section impedances in microstrip technology. The bandwidth of the filter can be significantly extended to cover the whole ultra wideband (UWB) frequency range with high adjustability. Moreover, a tunable bandnotch is introduced within the filter response, which can be arbitrarily placed according to the required application. Varactor and PIN diodes are also utilized to facilitate a high tuning capability throughout the different filter characteristics with respect to bandwidth, center frequency, and bandnotch frequency. Based on the symmetry of the filter, even-odd mode analysis is applied to investigate the different filter design characteristics. In addition, a comprehensive transmission line model is investigated within this paper which showed excellent agreements with full-wave simulations and measurements. The implemented UWB filter is investigated with respect to its frequency-domain characteristics and group delay response. The realized filter has a fractional bandwidth of more than 119% with a low group delay. All measured results are in a very good agreement with analysis and simulations. The overall filter dimensions, including housing, do not exceed 25 mm×25 mm.

INDEX TERMS Bandpass filter (BPF), p-i-n diodes, ring resonator, ultra-wideband (UWB), varactors.

I. INTRODUCTION

The Federal Communications Commissions (FCC) has fixed the Ultra-Wideband (UWB) range for unlicensed use [1]. Since then, UWB transmission systems have been of a great interest for several low-power broadband communications applications. Based on these facts, UWB modules and circuits, particularly bandpass filters, become attractive to the wireless communication community. Several interesting designs and investigations have been there for more than a decade [2]–[5]. Most of them, however, are based on the multi-mode resonators which were originally proposed and introduced by Zhu *et al.* in [2].

Ring resonators are among the successful candidates in designing UWB filters due to their compact geometry and design simplicity [6]–[8]. They have demonstrated a long history of success starting the remarkable work of Ishida and Araki in [9] where they introduced an UWB filter composed of multiples of ring resonators. However, other attempts have been recently proposed and discussed different design configurations as well [10]–[14]. However, not all of these ring filter designs are capable of covering the whole UWB while introducing reasonable insertion loss values.

Electronically tunable and reconfigurable filter structures have been proposed by several authors [15]–[20]. They offer a wide range of applications and operation scenarios, such as mobile communication systems and emerging multi-band multi-purpose transceivers. They are featured by their low production costs and the efficient use of radio spectrum. However, not all of these solutions are capable of providing several tuning functions at the same time while maintaining a miniaturized size that fits modern wireless systems.

We propose a new class of tunable UWB filters based on a band-notched multi-mode ring resonator design [21]. Such filters can be arbitrary tuned and reconfigured with respect to their passband and bandnotch characteristics with the simultaneous use of varactor and PIN diodes. The ring resonators

proposed in this paper succeeded in providing multiple tuning capabilities in addition to their highly-miniaturized size and cost-effective fabrication. The filter response can be arbitrary synthesized using optimization techniques or during operation using electronic diode elements. Comprehensive analytical methods and Transmission Line Models (TLM) are also introduced which can be programmed into modern CAD tools. All of these features make them attractive for modern communications applications.

This manuscript is organized as follows: In the next section, the basic theory of the proposed multi-mode microstrip ring resonator is discussed. In section 3, the tuning capabilities of the filter are illustrated along with a comprehensive model that is successfully employed within the design process. Such model takes into consideration the circuit models of the utilized varactor and PIN diodes with a higher accuracy and a real simplicity. The final section of this manuscript demonstrates the experimental results of the final reconfigurable UWB filter along with discussions.

II. THE PROPOSED MULTI-MODE RING RESONATOR

The basic element of the filter design is the multi-mode ring resonator shown in Fig. 1a. This resonator is an orthogonally-fed microstrip ring structure which can also be implemented on any other planar technology. The ring is constructed of four different sections as shown in the same figure. Each section has a variable width that corresponds to a different characteristic impedance. A direct connection between the I/O ports is additionally formed through a 90° microstrip bend.

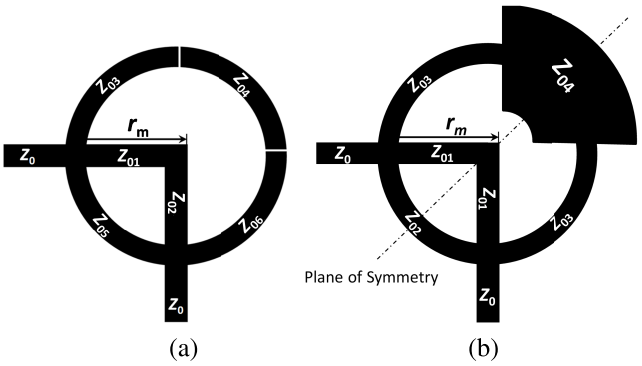

FIGURE 1. The proposed multi-mode stepped-impedance ring resonator. (a) Generalized case. (b) Symmetric case.

According to the theory of dual-mode ring resonators [20], a ring resonator can accommodate two degenerate resonance modes if a perturbation is introduced at its plane of symmetry. Such perturbation can be a gap, a short-circuited via or a section with a different characteristic impedance. Fig. 1b depicts the modified version of the generalized structure of the ring where the characteristic impedance of the upper right-handed section is made significantly smaller than the rest of the ring to provide such perturbation. Moreover, the direct transmission line between the I/O ports through the 90° bend is intended to introduce a third mode which makes the overall structure acts like a triple-mode resonator. The ring can accommodate multi-modes if each quarter has a different characteristic impedance which can be considered, in such case, a stepped-impedance resonator [13]. The ring will resonate if the guided wavelength λ_g is multiples of its perimeter as

$$2\pi r_m = n\lambda_g \tag{1}$$

where r_m is the mean radius of the ring and n is the resonance mode. This equation declares that the fundamental resonance occurs whenever the guided wavelength is equal to the perimeter of the ring.

A. EVEN-ODD MODE ANALYSIS

The even-odd mode analysis of the simplified filter structure was presented by the authors in a previous publication where all sections had the same characteristic impedance [21]. The generalized symmetric structure, shown in Fig. 1b, is analyzed here. Each arc length of the ring is related to its mean radius r_m at resonance as

$$\begin{aligned} l_{01} &= r_m, \\ l_{02} &= \frac{\pi r_m}{4}, \\ l_{03} &= \frac{\pi r_m}{2}, \\ l_{04} &= \frac{\pi r_m}{4}. \end{aligned} \tag{2}$$

where l_{0n} corresponds to the length of the arc whose characteristic impedance is Z_{0n}.

The even-mode circuit is shown in Fig. 2a where all derivations are performed in the admittance domain. Each individual input admittance is evaluated according to

$$Y_1^e = jY_{01}\tan\left(\frac{\lambda_g}{\lambda}\right) \tag{3}$$

$$Y_2^e = jY_{02}\tan\left(\frac{\pi\lambda_g}{4\lambda}\right) \tag{4}$$

$$Y_3^e = Y_{03}\frac{Y_4^e + jY_{03}\tan\left(\frac{\pi\lambda_g}{2\lambda}\right)}{Y_{03} + jY_4^e\tan\left(\frac{\pi\lambda_g}{2\lambda}\right)} \tag{5}$$

where

$$Y_4^e = jY_{04}\tan\left(\frac{\pi\lambda_g}{4\lambda}\right) \tag{6}$$

As for the odd-mode circuit shown in Fig. 2b, the resulting input admittance can be evaluated in the same way. The input admittance of both modes can be determined as

$$Y_{even} = Y_1^e + Y_2^e + Y_3^e \tag{9}$$

$$Y_{odd} = Y_1^o + Y_2^o + Y_3^o \tag{10}$$

This will result into the expressions of the even- and odd-mode characteristic admittances of (9) and (10). These two equations can be utilized to determine the resonant frequency

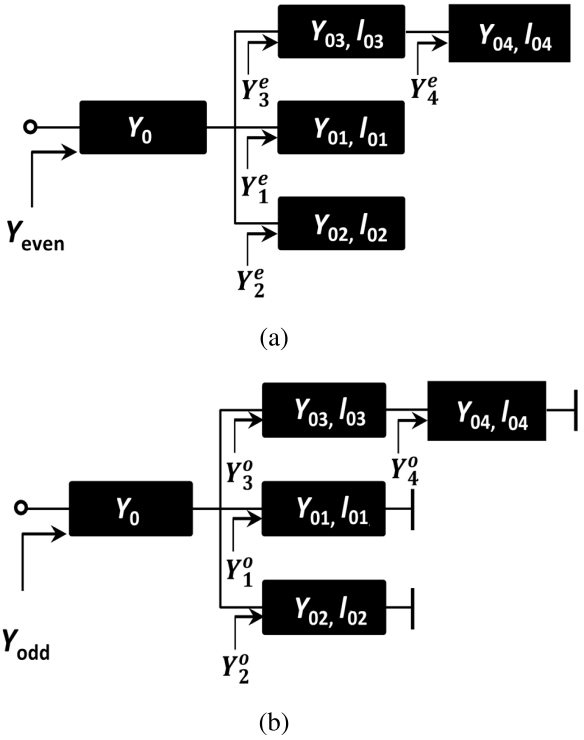

FIGURE 2. Even-Odd mode analysis of the ring resonator. (a) Even-Mode circuit. (b) Odd-Mode circuit.

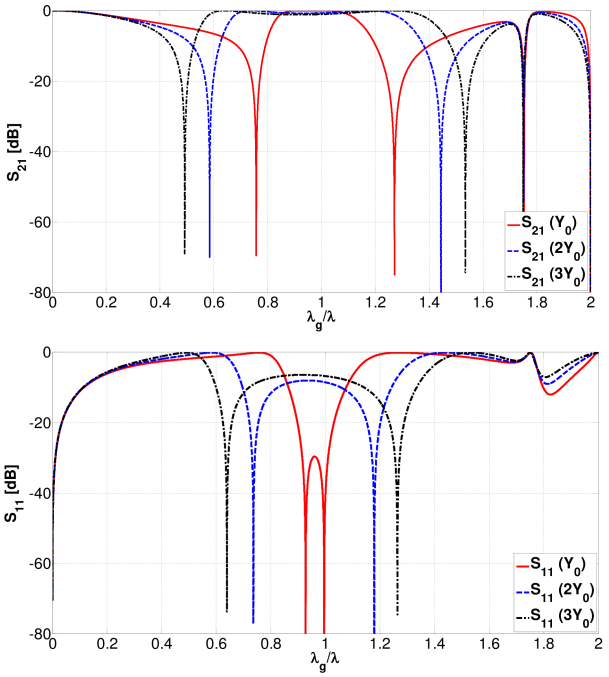

FIGURE 3. Calculated *S*-parameters of the proposed multi-mode resonator at different characteristic admittance states.

of the resonator at zero input admittance as a closed-form or a graphical solution.

The even-mode reflection coefficient Γ_{even} scaled to the overall system characteristic admittance Y_0 is given by

$$\Gamma_{even} = \frac{Y_0 - Y_{even}}{Y_0 + Y_{even}} \tag{11}$$

Similarly, The odd-mode reflection coefficient Γ_{odd} will be

$$\Gamma_{odd} = \frac{Y_0 - Y_{odd}}{Y_0 + Y_{odd}} \tag{12}$$

Both the return loss S_{11} and the insertion loss S_{21} of the filter can be directly determined according to

$$S_{11} = \frac{\Gamma_{even} + \Gamma_{odd}}{2} \tag{13}$$

$$S_{21} = \frac{\Gamma_{even} - \Gamma_{odd}}{2} \tag{14}$$

and this completes the even-odd mode analysis of the filter.

Equations (9) and (10) are used here to investigate the dual-mode filter characteristics and resonance conditions. As shown in Fig. 3, the characteristic admittance of the upper right section of the filter Y_{04} is made variable while all other resonator sections are kept constant at Y_0. It is clear from the figure that, the bandwidth significantly increases as the characteristic admittance of this section increases. The scattering parameters are plotted here against λ_g/λ which is nothing but a direct mapping of the frequency-domain into the wavelength-domain. The figure shows three different plots of both S_{11} and S_{21} at three different Y_{04} states, namely ($Y_{04} = Y_0$, $Y_{04} = 2Y_0$ and $Y_{04} = 3Y_0$). However, varying the characteristic admittance with other filter sections also had a direct influence on bandwidth tuning. Since the frequency and wavelength are inversely proportional, this figure directly implies that the bandwidth of the filter increases as the characteristic impedance of the upper right section decreases. It can be observed that the higher the bandwidth, the higher the mismatch loss within the passband which is definitely the

$$Y_{even} = jY_{01}\tan\left(\frac{\lambda_g}{\lambda}\right) + jY_{02}\tan\left(\frac{\pi\lambda_g}{4\lambda}\right) + Y_{03}\frac{jY_{04}\tan\left(\frac{\pi\lambda_g}{4\lambda}\right) + jY_{03}\tan\left(\frac{\pi\lambda_g}{2\lambda}\right)}{Y_{03} - Y_{04}\tan\left(\frac{\pi\lambda_g}{4\lambda}\right)\tan\left(\frac{\pi\lambda_g}{2\lambda}\right)} \tag{7}$$

Similarly

$$Y_{odd} = -jY_{01}\cot\left(\frac{\lambda_g}{\lambda}\right) - jY_{02}\cot\left(\frac{\pi\lambda_g}{4\lambda}\right) + Y_{03}\frac{-jY_{04}\cot\left(\frac{\pi\lambda_g}{4\lambda}\right) + jY_{03}\tan\left(\frac{\pi\lambda_g}{2\lambda}\right)}{Y_{03} + Y_{04}\cot\left(\frac{\pi\lambda_g}{4\lambda}\right)\tan\left(\frac{\pi\lambda_g}{2\lambda}\right)} \tag{8}$$

cost of a greater bandwidth. Moreover, the filter possess sharp and selective passband characteristics.

B. HIGHER-ORDER FILTER STRUCTURE

Another interesting feature of the proposed bandpass filter is the capability of synthesizing even sharper and wider passband with much less insertion loss. By using a cascade of two or more identical rings as shown in Fig. 4, such feature can be implemented. This structure realizes a typical higher-order filter topology.

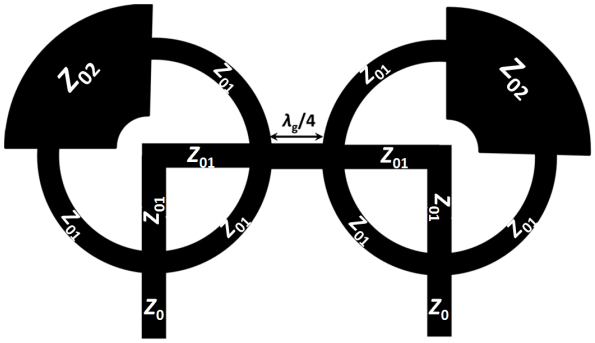

FIGURE 4. A cascaded higher-order filter structure.

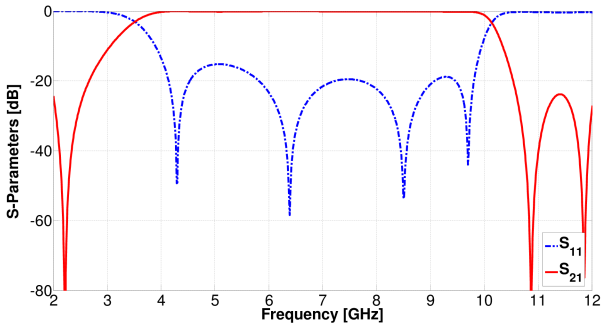

FIGURE 5. ADS simulated *S*-parameters of the cascaded filter.

The UWB filter structure is constructed of two identical ring resonators. Each section has a characteristic impedance Z_{01} except for the upper right section which has a different impedance Z_{02}. Both filters are separated by a $\lambda_g/4$ short transmission line section calculated with respect to the higher band edge. The simulated results of such cascaded filter structure are shown in Fig. 5. These results are simulated using ADS schematic where an excellent UWB response is achieved. The passband ripples are below 16-18 dB and the insertion loss value does not exceed 0.13 dB over the whole UWB frequency. This schematic simulation assumes ideal transmission line structures.

III. FILTER TUNING CAPABILITIES

In addition to the previously-investigated tunable filter structure with variable impedance sections, a comprehensive topology that employs varactor and PIN diodes is discussed in this section. The main function of such diode elements is to provide a higher degree-of-freedom in tuning the filter response with respect to its bandwidth, center frequency and for introducing an arbitrary bandnotch. Some recent UWB band-notched filter structures can be found in literature [22]–[24].

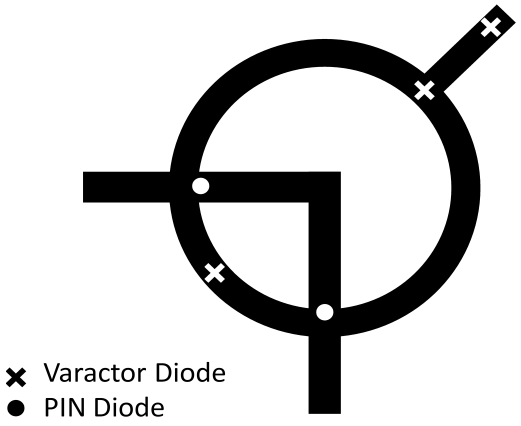

FIGURE 6. Possible placing positions for the varactor and PIN diodes.

The schematic diagram of possible placements for the varactor and PIN diodes is shown in Fig. 6. After analyzing and investigating the tunable filter structure, the following can be concluded:

- By placing a pair of PIN diodes at the slots S_2 (see Fig. 7), this will switch the additional resonance mode caused by the 90° bend path and consequently widens or narrows the bandwidth.
- By placing a varactor diode on the plane of symmetry, either in the upper or the lower quarter of the ring, this will help in tuning the second degenerate mode of the dual-mode operation and consequently will control the center frequency and/or the bandwidth of the filter.
- By adding a quarter-wave stub loaded with a varactor diode, this will introduce an arbitrary bandnotch that can be tunable by the varactor diode biasing voltage.

The realized reconfigurable filter structure is shown in Fig. 7. Each parameter of this filter is stated and defined in Table I.

In order to intensively investigate the tuning capabilities of the proposed filter, the transmission line model of the overall structure is analyzed next.

A. COMPREHENSIVE TRANSMISSION LINE MODEL

The model proposed by Wang *et al.* [18] is employed here with some modifications and extensions to cover all filter elements and components. As shown in Fig. 8, the model consists of three shunt branches; two of them represent the upper and the lower parts of the ring, denoted as (UR) and (LR), respectively. The middle ring (MR) branch models the two PIN diodes connected to the 90° microstrip bend. In this case, the bend is subdivided into two separate short transmission lines so as to facilitate modeling different characteristic impedances which is the unique property of the filter.

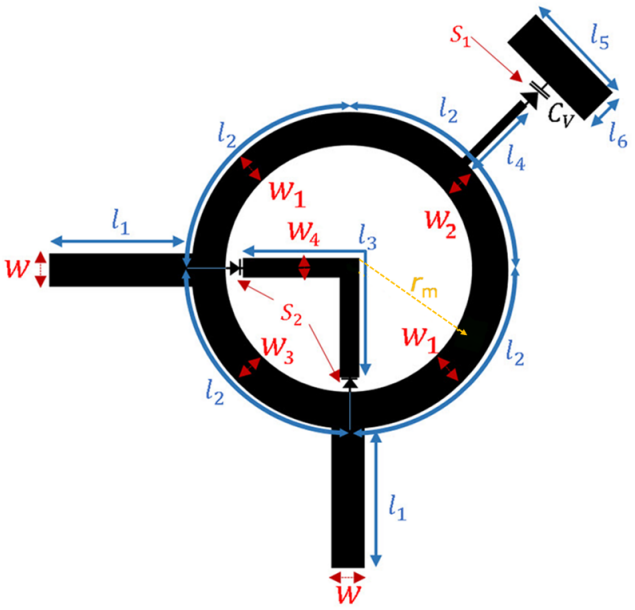

FIGURE 7. Schematic diagram of the realized UWB tunable filter structure.

TABLE 1. Realized Filter Parameters

Parameter	Definition	Dimension (mm)
W	50Ω line width	1
W_1	Arc width	0.21
W_2	Arc width	2.5
W_3	Arc width	0.25
W_4	90° Bend width	0.5
r_m	Mean radius of the ring	4
l_1	50Ω line length	8
l_2	Arc length	6.28
l_3	90° Bend length	5.66
l_4	Stub length	5
l_5	Varactor bias: stub width	3.75
l_6	Varactor bias: stub length	2
S_1	Slot width: Varactor diode	1.12
S_2	Slot width: PIN diodes	0.8

The model starts with partitioning the ring structure into smaller elements; each element is modeled by a microstrip curvature and a short transmission line section. The curvature of the ring is modeled by an *LC* T-network where the *LC* values are calculated based on the curvature angle and the characteristic impedance calculations of microstrip lines [27]. It is then combined with a short transmission line section that is modeled by another T-network of two impedances Z_a and Z_b according to Richard's transformation [26]. Both the varactor and the PIN diodes are modeled based on their equivalent lumped circuit model provided by the manufacturer [25].

Fig. 9a shows the equivalent circuit model of the varactor diode (Skyworks SMV1234) employed in this work. The elements L_S and R_S are the series inductance and resistance, respectively. The shunt capacitance C_P stands here for the packaging capacitance. The diode variable capacitance C_V represents the reverse-biased diode capacitance which ranges from 1.32 pF up to 9.63 pF. The overall varactor diode impedance Z_{var} is given in (18) and is included in the comprehensive filter model.

$$Z_{var} = \frac{\left(R_S + \frac{1}{j\omega C_V}\right) \cdot \frac{1}{j\omega C_S}}{R_S + \frac{1}{j\omega C_V} + \frac{1}{j\omega C_S}} + j\omega L_S \tag{18}$$

The equivalent circuit models of the 'ON' and 'OFF' states of the PIN diode (Skyworks SMP1352) are shown in Fig. 9b. The inductance L represents the parasitic inductance of the diode packaging. The capacitance C_T and the resistance R_D model the reverse-biased junction parameters. Likewise, the overall impedance of the recerse-biased PIN diode is included in the model as stated in (19).

$$Z_{pin} = \frac{\frac{R_D}{j\omega C_T}}{R_D + \frac{1}{j\omega C_T}} + j\omega L \tag{19}$$

The overall model is now segmented into subsections according to the declarations made above. The upper branch of the ring will be expanded into the *ABCD* chain in (15)-(17), are shown at the bottom of this page. This equation consists of the *ABCD* matrix of 3/4-ring that is composed of the microstrip curvature (C) and the short TL section (T) which have been partitioned into 134 segments in order to increase calculations accuracy. The *ABCD* matrix of the varactor is also included in the overall cascaded upper ring branch as evaluated in (15).

The middle branch is composed of the PIN diode matrices in addition to both TL sections of the 90° bend. The TL equivalent model is represented by the impedances Z_{at} and Z_{bt}, which can be variable according to the chosen characteristic

$$\begin{bmatrix} A & B \\ C & D \end{bmatrix}_{UR} = \left(\begin{bmatrix} A & B \\ C & D \end{bmatrix}_T \cdot \begin{bmatrix} A & B \\ C & D \end{bmatrix}_C \right)^{134} \cdot \begin{bmatrix} A & B \\ C & D \end{bmatrix}_{var} \cdot \left(\begin{bmatrix} A & B \\ C & D \end{bmatrix}_C \cdot \begin{bmatrix} A & B \\ C & D \end{bmatrix}_T \right)^{134} \tag{15}$$

$$\begin{bmatrix} A & B \\ C & D \end{bmatrix}_{MR} = \begin{bmatrix} A & B \\ C & D \end{bmatrix}_{pin} \cdot \begin{bmatrix} A & B \\ C & D \end{bmatrix}_{TL} \cdot \begin{bmatrix} A & B \\ C & D \end{bmatrix}_{TL} \cdot \begin{bmatrix} A & B \\ C & D \end{bmatrix}_{pin} \tag{16}$$

$$\begin{bmatrix} A & B \\ C & D \end{bmatrix}_{LR} = \left(\begin{bmatrix} A & B \\ C & D \end{bmatrix}_T \cdot \begin{bmatrix} A & B \\ C & D \end{bmatrix}_C \right)^{44} \tag{17}$$

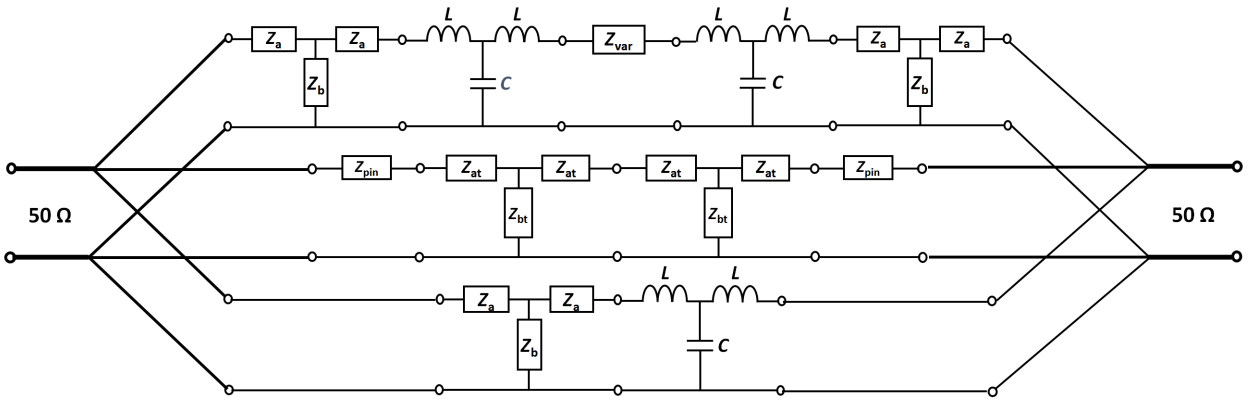

FIGURE 8. Comprehensive transmission line model of the overall filter structure including PIN and varactor diode elements.

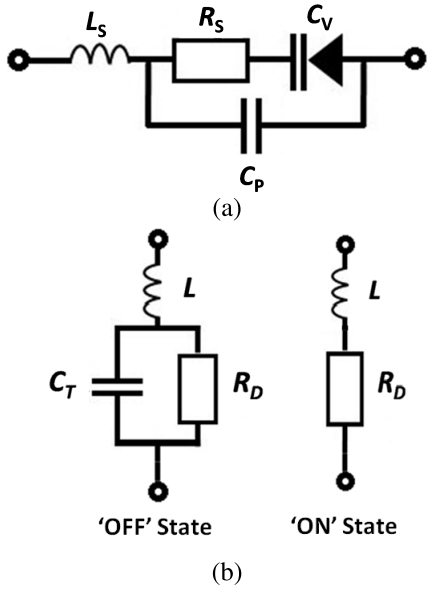

FIGURE 9. Circuit models of the diodes utilized in filter tuning. (a) Varactor diode. (b) PIN diode in both switching states.

impedance values. Similar to (15), the lower part of the ring (LR) is modeled in (17) but with 44 segments in this case.

Since the three branches are in a shunt arrangement, it will be reasonable to convert their *ABCD* matrices into the corresponding *Y*-matrices in order to sum them up. Equations (20)-(22) are the direct conversion of the *ABCD* into the *Y*-parameters.

$$\begin{bmatrix} Y_{11} & Y_{12} \\ Y_{21} & Y_{22} \end{bmatrix}_{UR} = \begin{bmatrix} \frac{D}{B} & \frac{BC-AD}{B} \\ \frac{-1}{B} & \frac{A}{B} \end{bmatrix}_{UR} \tag{20}$$

$$\begin{bmatrix} Y_{11} & Y_{12} \\ Y_{21} & Y_{22} \end{bmatrix}_{MR} = \begin{bmatrix} \frac{D}{B} & \frac{BC-AD}{B} \\ \frac{-1}{B} & \frac{A}{B} \end{bmatrix}_{MR} \tag{21}$$

$$\begin{bmatrix} Y_{11} & Y_{12} \\ Y_{21} & Y_{22} \end{bmatrix}_{LR} = \begin{bmatrix} \frac{D}{B} & \frac{BC-AD}{B} \\ \frac{-1}{B} & \frac{A}{B} \end{bmatrix}_{LR} \tag{22}$$

Thus, the equivalent *Y*-matrix of the overall ring will be the summation of the three *Y*-matrices.

$$[Y]_{Ring} = [Y]_{UR} + [Y]_{MR} + [Y]_{LR} \tag{23}$$

This completes the comprehensive modeling process of the tunable filter structure.

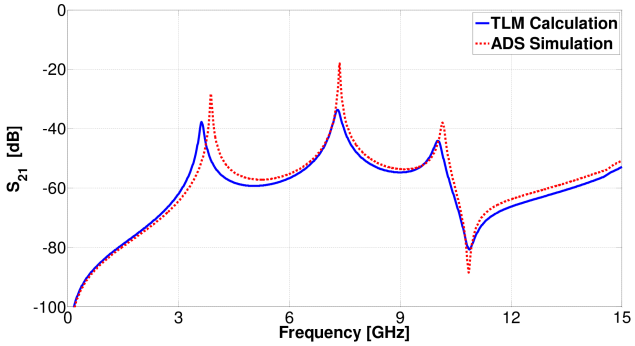

FIGURE 10. Calculated and simulated results of the loosely-coupled UWB triple-mode resonator.

In order to validate this model, intensive ADS simulations were performed and showed a perfect agreement with the proposed model. Fig. 10 shows the S_{21} response of the filter under loose coupling conditions compared to ADS simulations. The response shown here indicates a triple-mode operation that covers the whole UWB range where all the calculated resonance frequencies are identical to simulations.

Another interesting feature of the filter is illustrated in Fig. 11; by switching both PIN diodes on/off, the corresponding resonance mode appears/disappears, respectively. This feature can help in controlling the filter bandwidth significantly. Another alternative is to control the resonance frequency of any of the modes. Such example is shown in Fig. 12 where the varactor diode is utilized to move the resonant mode of the 3 GHz frequency. An excellent agreement between all TLM model calculations and ADS simulations can still be observed.

The dimensions of the final UWB optimized bandpass filter of the schematic design, shown in Fig. 7, are stated in Table I where its measured results are discussed in the next section. The detailed design process of the reconfigurable filter is depicted in the flowchart of Fig. 13.

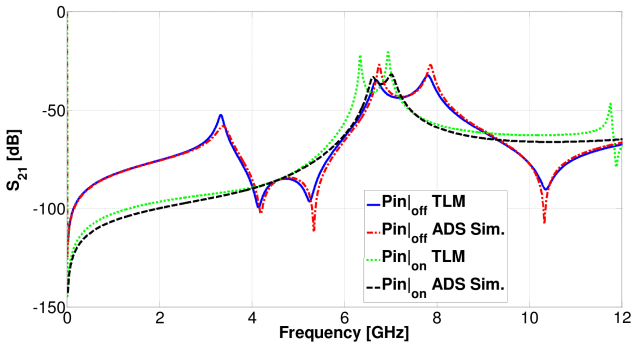

FIGURE 11. Calculated and simulated results of the PIN diode tuning capability.

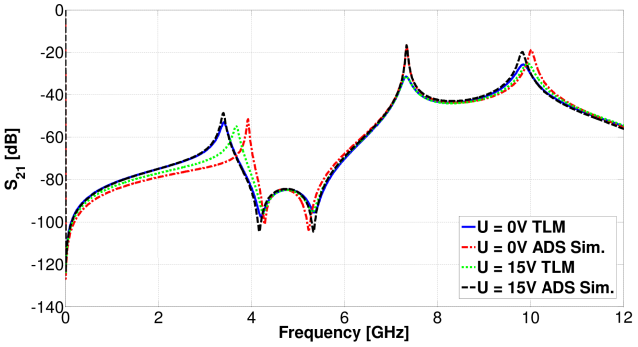

FIGURE 12. Calculated and simulated results of the varactor diode tuning capability.

IV. EXPERIMENTAL RESULTS

All measurements are performed using Agilent E8361A vector network analyzer. Calibration process is carried out using the electronic calibration module (Agilent E-Cal N4694). A photograph of the fabricated UWB tunable filter prototype is shown in Fig. 14. The filter is implemented on Rogers RO4003C substrate with a dielectric constant of 3.5, a loss tangent of 0.0027 and a substrate thickness of 0.51 mm. The DC supply to the varactor and the PIN diodes is provided through three low-pass filters. Two of them are supplying both the varactor and the PIN diodes while the third is supplying a 0V to the ground. This solution has proven its efficiency in suppressing flickers and distortions in the measured response due to cable parasitics. There are two additional blocking capacitors with the values (10 pF and 1 nF) connected to the feeding points for further signal quality enhancement.

The measured scattering parameters of the filter are shown in Fig. 15. The bias voltage for the PIN diode is 30V while it is 15V for the varactor diode to attain the desired response. The mounted varactor and PIN diodes are modeled on CST by their SPICE model parameters obtained from their datasheets [25]. As for the PIN diode, the "ON" state is modeled by the equivalent parameters of its maximum bias voltage while the "OFF" state is modeled by the parameters of the unbiased circuit. A reasonably good agreement between CST Microwave Studio simulations and measurements can be observed. The return loss values do not exceed 15.58 dB as depicted in the same figure. The insertion loss is somewhat higher due to the existing losses of both diodes which significantly contribute to the overall filter losses. The two band edges of the filter are at 3.36 GHz

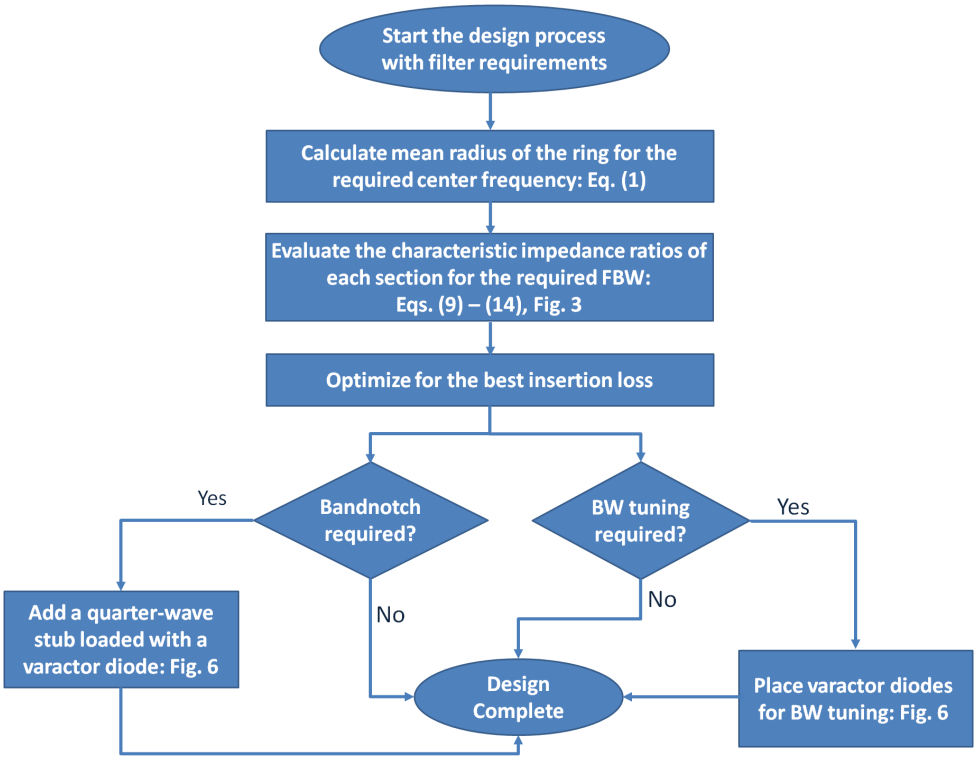

FIGURE 13. Detailed design process of the reconfigurable filter.

TABLE 2. A comparison between the proposed filter and other contributions.

Ref.	Substrate (ε_r/h)	FBW (%)	RL (dB)	Tunability	Size	Group Delay (ns)
[4]	2.45/0.8	108	13	N.A.	19×14	N.A.
[5]	2.3/0.5	115	10	N.A.	16.6×13	N.A.
[22]	2.33/0.79	110	11	N.A.	32.4×26.7	0.4
[23]	2.2/0.787	108	10	N.A.	11.25×4.8	N.A.
[24]	3.38/0.508	111	11	BN	15.2×14.5	0.4
This Work	**3.5/0.51**	**119**	**15.58**	**PB+BN**	**25×25**	**0.26**

All dimensions are in mm. RL: Return Loss, PB: Passband, BN: Bandnotch.

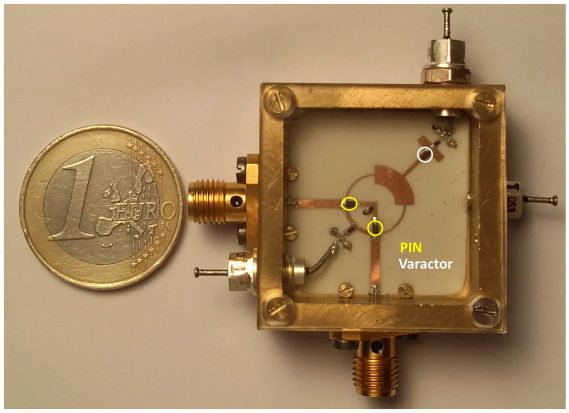

FIGURE 14. A photograph of the implemented UWB tunable filter.

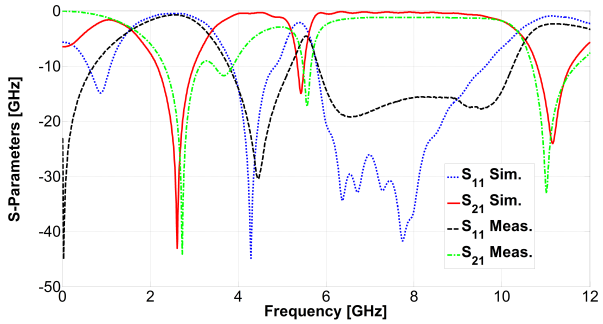

FIGURE 15. Measured and simulated *S*-parameters of the UWB tunable filter.

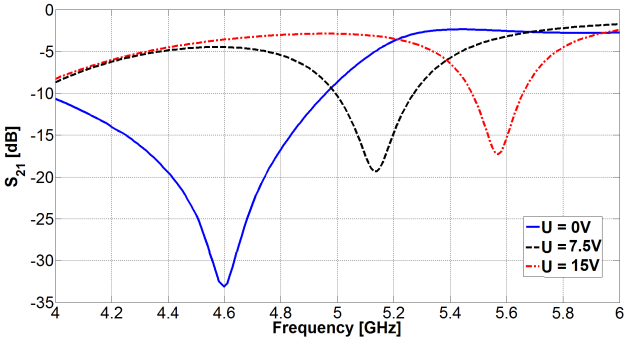

FIGURE 16. Measured values of the tunable bandnotch frequencies versus applied varactor voltages.

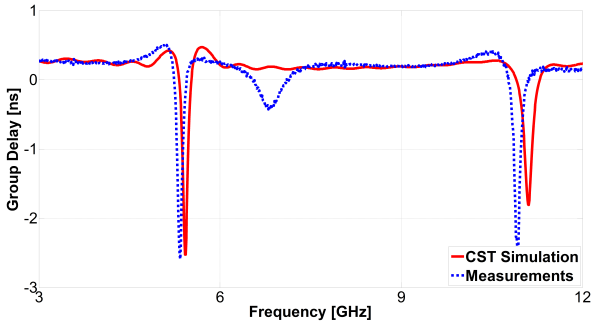

FIGURE 17. Measured and simulated group delay response of the implemented UWB filter.

and 10.53 GHz which makes a 119% fractional bandwidth (FBW). A bandnotch of 5.56 GHz is attained by adjusting the biasing conditions of the varactor diode accordingly. Fig. 16 depicts the measured tuning range of the bandnotch frequency. By varying the bias voltage from 0 to 15V the notch frequency changes from 4.6 GHz to 5.6 GHz. However, it should be stressed on the fact that this filter can support higher tuning range which was proven previously by Kheir *et al.* [21]. Furthermore, the group delay response of the filter is shown in Fig. 17 where an excellent agreement with CST simulations can also be observed. The group delay does not exceed 0.26 ns within the passband which guarantees a reliable signal transmission over the whole UWB.

A comparison between the proposed filter specifications and other significant contributions is stated in Table II.

V. CONCLUSIONS

Throughout this manuscript, the design and implementation of novel UWB bandpass ring filters have been demonstrated. It has been shown that such filters can be equally modeled using both even-odd mode analysis or transmission line methods. A comprehensive TLM has been developed where it has proven its efficiency. This model could successfully accommodate diode models with a higher accuracy as well. Analytical results have shown excellent agreements with ADS and CST simulations. PIN and varactor diodes have been introduced for tuning purposes where they could

successfully control the center frequency, bandwidth and bandnotch frequency. Due to the higher FBW of the realized filter, which exceeded 119%, the utilized diodes have introduced additional losses. This can, however, be overcome if proper low-loss diodes have been selected. The measured response of the final filter structure has shown reasonably good characteristics with respect to its insertion loss and flat group delay which did not exceed 0.26 ns. Such new class of UWB filters can be a potential candidate for several UWB transmission and wireless communication applications that require higher selectivity and various tuning capabilities. Meanwhile, compact size and cost-effective implementation on conventional microstrip technology are maintained.

ACKNOWLEDGMENTS

The authors wish to sincerely thank the Associate Editor, Dr. Andrei Muller, and the reviewers for their helpful comments and discussions.

REFERENCES

[1] "Revision of part 15 of the commission's rules regarding ultrawideband transmission systems," Fed. Commun. Commission, Washington, DC, USA, Tech. Rep. ET-Docket 98-153, FCC02-48, 2002.
[2] L. Zhu, S. Sun, and W. Menzel, "Ultra-wideband (UWB) bandpass filters using multiple-mode resonator," *IEEE Microw. Wireless Compon. Lett.*, vol. 15, no. 11, pp. 796–798, Nov. 2005.
[3] Y. Zhou, B. Yao, Q. Cao, H. Deng, and X. He, "Compact UWB bandpass filter using ring open stub loaded multiple-mode resonator," *Electron. Lett.*, vol. 45, no. 11, pp. 554–556, May 2009.
[4] X. Li and X. Ji, "Novel compact UWB bandpass filters design with cross-coupling between μ/4 short-circuited stubs," *IEEE Microw. Wireless Compon. Lett.*, vol. 24, no. 1, pp. 23–25, Jan. 2014.
[5] A. Taibi, M. Trabelsi, A. Slimane, M. T. Belaroussi, and J. P. Raskin, "A novel design method for compact UWB bandpass filters," *IEEE Microw. Wireless Compon. Lett.*, vol. 25, no. 1, pp. 4–6, Jan. 2015.
[6] S. Hashemi and D. Mirshekar-Syahkal, "Ultra compact filters for ultra-wideband (UWB) applications using multilayer ring resonators," in *Proc. IEEE Int. Conf. Ultra-Wideband (ICUWB)*, Sep. 2009, pp. 516–520.
[7] C. H. Kim and K. Chang, "Ultra-wideband (UWB) ring resonator bandpass filter with a notched band," *IEEE Microw. Wireless Compon. Lett.*, vol. 21, no. 4, pp. 206–208, Apr. 2011.
[8] W. Feng, W. Che, and Q. Xue, "Compact ultra-wideband bandpass filters with narrow notched bands based on a ring resonator," *IET Microw., Antennas Propag.*, vol. 7, no. 12, pp. 961–969, Sep. 2013.
[9] H. Ishida and K. Araki, "Design and analysis of UWB band pass filter with ring filter," in *IEEE MTT-S Int. Microw. Symp. Dig.*, vol. 3. Jun. 2004, pp. 1307–1310.
[10] H. Zhu and Q.-X. Chu, "Ultra-wideband bandpass filter with a notch-band using stub-loaded ring resonator," *IEEE Microw. Wireless Compon. Lett.*, vol. 23, no. 7, pp. 341–343, Jul. 2013.
[11] S. Sun and L. Zhu, "Wideband microstrip ring resonator bandpass filters under multiple resonances," *IEEE Trans. Microw. Theory Techn.*, vol. 55, no. 10, pp. 2176–2182, Oct. 2007.
[12] S. Luo, L. Zhu, and S. Sun, "Compact dual-mode triple-band bandpass filters using three pairs of degenerate modes in a ring resonator," *IEEE Trans. Microw. Theory Techn.*, vol. 59, no. 5, pp. 1222–1229, May 2011.
[13] M. Matsuo, H. Yabuki, and M. Makimoto, "Dual-mode stepped-impedance ring resonator for bandpass filter applications," *IEEE Trans. Microw. Theory Techn.*, vol. 49, no. 7, pp. 1235–1240, Jul. 2001.
[14] L. C. Lin, S. Yang, S. J. Sun, B. Wu, and C. H. Liang, "Ultra-wideband bandpass filter using multi-stub-loaded ring resonator," *Electron. Lett.*, vol. 50, no. 17, pp. 1218–1220, Aug. 2014.
[15] T. S. Martin, F. Wang, and K. Chang, "Electronically tunable and switchable filters using microstrip ring resonator circuits," in *IEEE MTT-S Int. Microw. Symp. Dig.*, May 1988, pp. 803–806.
[16] R. Gómez-García and A. C. Guyette, "Reconfigurable multi-band microwave filters," *IEEE Trans. Microw. Theory Techn.*, vol. 63, no. 4, pp. 1294–1307, Apr. 2015.
[17] J.-S. Hong, "Reconfigurable planar filters," *IEEE Microw. Mag.*, vol. 10, no. 6, pp. 73–83, Oct. 2009.
[18] F. Wang, K. Chang, S. Martin, and J. L. Klein, "On the study of microstrip ring and varactor-tuned ring circuits," *IEEE Trans. Microw. Theory Techn.*, vol. 35, no. 12, pp. 1288–1295, Dec. 1987.
[19] J. A. Navarro and K. Chang, "Varactor-tunable uniplanar ring resonators," *IEEE Trans. Microw. Theory Techn.*, vol. 41, no. 5, pp. 760–766, May 1993.
[20] K. Chang and L.-H. Hsieh, *Microwave Ring Circuits and Related Structures*, 2nd ed. Hoboken, NJ, USA: Wiley, 2004.
[21] M. Kheir, M. Höft, and R. Knöchel, "A new simple UWB ring filter with flexible band-notch characteristics," in *Proc. IEEE Int. Conf. Ultra-WideBand (ICUWB)*, Sep. 2014, pp. 341–344.
[22] S. Kumar, R. D. Gupta, and M. S. Parihar, "Multiple band notched filter using C-shaped and E-shaped resonator for UWB applications," *IEEE Microw. Wireless Compon. Lett.*, vol. 26, no. 5, pp. 340–342, May 2016.
[23] P. Sarkar, R. Ghatak, M. Pal, and D. R. Poddar, "High-selective compact UWB bandpass filter with dual notch bands," *IEEE Microw. Wireless Compon. Lett.*, vol. 24, no. 7, pp. 448–450, Jul. 2014.
[24] H. Wang, K.-W. Tam, S.-K. Ho, W. Kang, and W. Wu, "Design of ultra-wideband bandpass filters with fixed and reconfigurable notch bands using terminated cross-shaped resonators," *IEEE Trans. Microw. Theory Techn.*, vol. 62, no. 2, pp. 252–265, Feb. 2014.
[25] [Online]. Available: http://www.skyworksinc.com
[26] D. M. Pozar, *Microwave Engineering*, 4th ed. Hoboken, NJ, USA: Wiley, 2012.
[27] M. Kirschning and R. H. Jansen, "Accurate model for effective dielectric constant of microstrip with validity up to millimetre-wave frequencies," *Electron. Lett.*, vol. 18, no. 6, pp. 272–273, Mar. 1982.
[28] P. Benedek and P. Silvester, "Equivalent capacitances for microstrip gaps and steps," *IEEE Trans. Microw. Theory Techn.*, vol. 20, no. 11, pp. 729–733, Nov. 1972.

MOHAMED KHEIR was born in Cairo, Egypt, in 1977. He received the M.Sc. degree in communications technology from the University of Ulm, Ulm, Germany, in 2005, and the Ph.D. degree (Hons.) in information engineering and technology from the German University in Cairo, Egypt, in cooperation with Magdeburg University, Germany, in 2011. From 2012 to 2015, he was a Lecturer with the Chair of Microwave Engineering, University of Kiel, Germany, where he was involved in several research projects and lecturing duties. Since 2015, he has been an RF-Development Engineer with IMS Connector Systems GmbH, Germany, where he is responsible for design and development of high-speed and multichannel data connectors for mobile base stations and automotive applications.

His research interests include microwave measurement techniques, microwave/mm-wave integrated circuits and RF identification and security.

Dr. Kheir was a recipient of the Early Career Award at the 27th Conference in precision electromagnetic measurements in 2010.

THOMAS KROEGER was born in Wismar, Germany, in 1987. He received the M.Sc. degree in electrical and information engineering and business management from Christian-Albrechts-University of Kiel, Kiel, Germany in 2015.

Since 2016, he has been a Process Improvement Engineer with Bradken, Australia.

MICHAEL HÖFT received the Dipl.-Ing. degree in electrical engineering and the Dr.-Ing. degree from the Hamburg University of Technology, Hamburg, Germany, in 1997 and 2002, respectively. From 2002 to 2013, he was with the Communications Laboratory, European Technology Center, Panasonic Industrial Devices Europe GmbH, Lüneburg, Germany, where he was a Research Engineer and then a Team Leader, where he was involved in the research and development of microwave circuitry and components, particularly filters for cellular radio communications. From 2010 to 2013, he had also been a Group Leader for the research and development of sensor and network devices. Since 2013, he has been a Full Professor with the Faculty of Engineering, University of Kiel, Kiel, Germany, where he is currently the Head of the Chair for Microwave Engineering, Institute of Electrical and Information Engineering. His research interests include active and passive microwave components, (sub) millimeter-wave quasi-optical techniques and circuitry, microwave and field measurement techniques, microwave filters, microwave sensors, and magnetic field sensors. He is a member of the European Microwave Association, the Association of German Engineers, and a member of the German Institute of Electrical Engineers.